

# EARLY OBSERVATIONS OF THE TYPE IA SUPERNOVA iPTF 16abc: EVIDENCE FOR STRONG EJECTA MIXING AND/OR INTERACTION WITH DIFFUSE MATERIAL

A. A. MILLER,<sup>1,2</sup> Y. CAO,<sup>3</sup> A. L. PIRO,<sup>4</sup> N. BLAGORODNOVA,<sup>5</sup> B. D. BUE,<sup>6</sup> S. B. CENKO,<sup>7,8</sup> S. DHAWAN,<sup>9</sup> R. FERRETTI,<sup>9</sup>  
O. D. FOX,<sup>10</sup> C. FREMLING,<sup>11</sup> A. GOOBAR,<sup>9</sup> D. A. HOWELL,<sup>12,13</sup> G. HOSSEINZADEH,<sup>12,13,14</sup> M. M. KASLIWAL,<sup>5</sup>  
R. R. LAHER,<sup>15</sup> R. LUNNAN,<sup>5</sup> F. J. MASCI,<sup>15</sup> P. E. NUGENT,<sup>16,17</sup> J. SOLLERMAN,<sup>11</sup> F. TADDIA,<sup>11</sup> AND S. R. KULKARNI<sup>5</sup>

<sup>1</sup>*Center for Interdisciplinary Exploration and Research in Astrophysics (CIERA) and Department of Physics and Astronomy, Northwestern University, 2145 Sheridan Road, Evanston, IL 60208, USA*

<sup>2</sup>*The Adler Planetarium, Chicago, IL 60605, USA*

<sup>3</sup>*eScience Institute and Astronomy Department, University of Washington, Seattle, WA 98195*

<sup>4</sup>*The Observatories of the Carnegie Institution for Science, 813 Santa Barbara Street, Pasadena, CA 91101, USA*

<sup>5</sup>*Division of Physics, Mathematics, and Astronomy, California Institute of Technology, Pasadena, CA 91125, USA*

<sup>6</sup>*Jet Propulsion Laboratory, California Institute of Technology, Pasadena, CA 91109, USA*

<sup>7</sup>*NASA Goddard Space Flight Center, Mail Code 661, Greenbelt, MD 20771, USA*

<sup>8</sup>*Joint Space-Science Institute, University of Maryland, College Park, MD 20742, USA*

<sup>9</sup>*The Oskar Klein Centre, Department of Physics, AlbaNova, SE-106 91 Stockholm, Sweden*

<sup>10</sup>*Space Telescope Science Institute, 3700 San Martin Drive, Baltimore, MD 21218, USA*

<sup>11</sup>*The Oskar Klein Centre, Department of Astronomy, AlbaNova, SE-106 91 Stockholm, Sweden*

<sup>12</sup>*Las Cumbres Observatory, Goleta, CA 93117, USA*

<sup>13</sup>*Physics Department, University of California, Santa Barbara, CA 93106, USA*

<sup>14</sup>*LSSTC Data Science Fellow*

<sup>15</sup>*Infrared Processing and Analysis Center, California Institute of Technology, Pasadena, CA 91125, USA*

<sup>16</sup>*Lawrence Berkeley National Laboratory, Berkeley, California 94720, USA*

<sup>17</sup>*University of California – Berkeley, Berkeley, CA 94720, USA*

(Received August 9, 2017; Revised; Accepted)

Submitted to ApJ

## ABSTRACT

Early observations of Type Ia supernovae (SNe) provide a unique probe of their progenitor systems and explosion physics. Here, we report the intermediate Palomar Transient Factory (iPTF) discovery of an extraordinarily young SN Ia, iPTF 16abc. By fitting a power law to our early light curve, we infer that first light for the SN, that is when appreciable heating from <sup>56</sup>Ni decay has first diffused to the photosphere, only occurred  $0.15 \pm_{0.07}^{0.15}$  d before our first detection. In the  $\sim 24$  hr after discovery, iPTF 16abc rose by  $\sim 2$  mag, following a near-linear rise in flux for  $\sim 4$  d. Strong C II absorption is detected in the early spectra of iPTF 16abc, before disappearing after  $\sim 7$  d. Unlike SN 2011fe, the  $(B - V)_0$  colors of iPTF 16abc are blue and nearly constant in the days after explosion. We show that our early observations of iPTF 16abc cannot be explained by either SN shock breakout and the associated, subsequent cooling, or the SN ejecta colliding with a stellar companion. Instead, we argue that the early characteristics of iPTF 16abc, including: (i) the rapid, near-linear rise, (ii) the non-evolving blue colors, and (iii) the strong absorption from ionized carbon, are the result of either vigorous mixing of radioactive <sup>56</sup>Ni in the SN ejecta, or ejecta interaction with diffuse material, or a combination of the two. In the next few years, dozens of very young *normal* SNe Ia will be discovered, and observations similar to those presented here will constrain the white dwarf explosion mechanism.

*Keywords:* methods: observational — supernovae: general — supernovae: individual (iPTF 16abc)

## 1. INTRODUCTION

Although Type Ia supernovae (SNe Ia) have been extensively used as standardizable candles, their progenitor systems and explosion physics are still debated (see a recent review by Maoz et al. 2014). Extremely detailed observations in the hours to days after explosion provide a promising avenue to further constrain this problem.

While the shock breakout of a SN Ia occurs on a sub-second timescale, the subsequent quasi-adiabatic expansion and cooling of the unbound ejecta produces thermal emission that can be used to infer the radius of the exploding star (Piro et al. 2010; Rabinak & Waxman 2011). Comparing models of this cooling emission to the earliest-phase data of SN 2011fe, Bloom et al. (2012) concluded that the explosion came from a star with  $R_* \lesssim 0.02 R_\odot$ , where  $R_\odot$  is the solar radius. Combining the radius constraint with the measured ejecta mass, Bloom et al. derive the mean density of the progenitor star, confirming that at least some Type Ia SNe come from compact and degenerate stars.

Early phase observations of SNe Ia from a white dwarf (WD)+non-degenerate binary may detect excess emission, relative to most Type Ia SNe, due to the collision of the SN ejecta with the non-degenerate companion (Whelan & Iben 1973; Kasen 2010). This excess emission was first detected in iPTF 14atg (Cao et al. 2015), a low-velocity SN Ia with a significant and declining ultraviolet (UV) pulse detected within a few days of the SN explosion. This UV pulse is best interpreted as a SN ejecta-companion collision (but see also Kromer et al. 2016; Noebauer et al. 2017). While such emission requires a favorable geometric alignment and is only expected in  $\lesssim 10\%$  of SNe Ia (Kasen 2010), many studies have searched for signatures of an ejecta-companion interaction, typically resulting in non-detections (e.g., Hayden et al. 2010a; Bianco et al. 2011; Foley et al. 2012; Bloom et al. 2012; Olling et al. 2015; Zheng et al. 2013; Goobar et al. 2015; Shappee et al. 2016b; Im et al. 2015). Possible exceptions include SN 2012cg, which exhibited excess blue emission in its early-phase light curve (Marion et al. 2016; though see Shappee et al. 2016a for an interpretation that does not invoke ejecta-companion interaction), and SN 2017cbv, which shows a clearly resolved “bump” in the early  $UBg$  light curves (Hosseinizadeh et al. 2017).

Interaction is not limited to systems with a non-degenerate companion, however, as WDs enshrouded in diffuse material following a binary merger (e.g., Levanon et al. 2015) or expanded due to a pre-explosion pulsation can give rise to ejecta-interaction signatures (e.g., Dessart et al. 2014). Models of this scenario naturally produce C II absorption that is comparable in strength to Si II in the days after explosion (Dessart et al. 2014),

as was observed in SN 2013dy (Zheng et al. 2013) and SN 2017cbv (Hosseinizadeh et al. 2017).

The vast majority of SNe Ia are observed to be powered purely by the radioactive decay of  $^{56}\text{Ni}$ . While the detection of SN shock cooling or ejecta interaction is rare, the level of  $^{56}\text{Ni}$  mixing in the SN ejecta can fundamentally alter the appearance of the SN shortly after explosion. SNe Ia experience a dark phase after the SN shock breakout but before radioactive energy diffuses into the photosphere (Piro & Nakar 2014). The duration of this dark phase is set by how the newly synthesized  $^{56}\text{Ni}$  is mixed and deposited into different layers of the ejecta. In the case of strong mixing, the dark phase is short, or non-existent, as  $\gamma$ -rays from the radioactive  $^{56}\text{Ni}$  diffuse to the photosphere rapidly. This also leads to blue optical colors and a rapid initial rise in the observed light curve. If the mixing is weak and the  $^{56}\text{Ni}$  is confined to the innermost layers of the ejecta, the dark phase can last for several days as the radioactive energy diffuses to the photosphere. The early evolution of such SNe results in redder colors and a more moderate rise in luminosity (Piro & Morozova 2016). Thus, the early light curves of even non-exotic Type Ia SNe convey information about their progenitor systems by constraining the distribution of synthesized  $^{56}\text{Ni}$ , which in turn constrains the explosion mechanism.<sup>1</sup>

Noebauer et al. (2017) recently demonstrated that disambiguating between these different scenarios via optical photometry alone is challenging. Noebauer et al. further show that estimates of the time of explosion, which are critical for comparing models with observations, are often incorrect by as many as  $\sim 2$  d using common methods in the literature. While analytical models suggest that early spectra can be used to infer the time of explosion (e.g., Piro & Nakar 2014), more detailed simulations show that the photospheric evolution is not so simple (Piro & Morozova 2016). Reconciling these issues requires both a larger sample of early SNe Ia observations and more detailed models that produce synthetic light curves and spectra.

In this paper, we report observations of an extraordinarily young SN Ia, iPTF 16abc, which was discovered by the intermediate Palomar Transient Factory (iPTF) on 2016 April 3.36 UTC at R.A. =  $13^{\text{h}}34^{\text{m}}45.49^{\text{s}}$ , Dec. =  $+13^{\circ}51'14''3$  (J2000) with a  $g_{\text{PTF}}$ -band magnitude of  $21.31 \pm 0.27$  (Miller et al. 2016). The transient is spatially coincident with a tidal tail of the galaxy NGC 5221, which lies at a distance of  $\sim 100$  Mpc. iPTF 16abc is not detected to a limit of  $g = 22.1$  mag on

<sup>1</sup> Taddia et al. (2015) found that a significant dark phase is not prevalent for a sample of Type Ib/c SNe.

April 2.42, less than 1 d prior to discovery, and rose by  $\sim 2$  mag in the 24 hr following its initial detection. Our spectroscopic follow-up campaign classified iPTF 16abc as a normal SN Ia (Cenko et al. 2016). Our observations and analysis show that the early evolution of iPTF 16abc exhibited several distinct properties relative to SN 2011fe. We interpret those differences as arising from either strong  $^{56}\text{Ni}$  mixing or ejecta interaction with diffuse material, or a combination of the two.

## 2. OBSERVATIONS

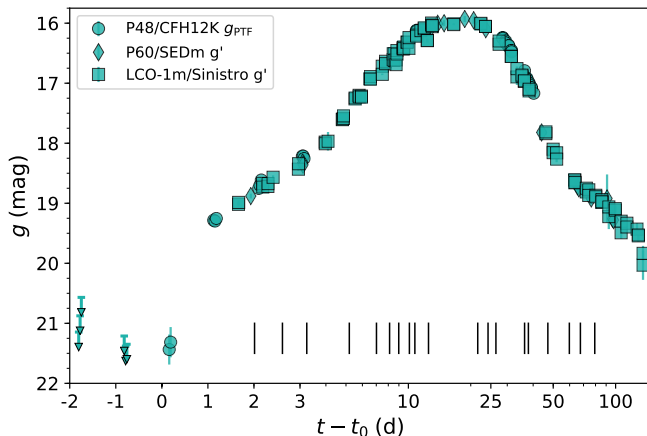


**Figure 1.** The  $g$ -band light curve of iPTF 16abc. Observations from different telescopes are shown with different symbols. Time is measured in rest-frame days relative to the time of first light,  $t_0$  (see §4.1). Note that the horizontal axis is shown with a linear scale for  $-2 \text{ d} \leq t - t_0 \leq 3 \text{ d}$  and a log scale for  $t - t_0 > 3 \text{ d}$ . The black ticks near the bottom of the panel show epochs of spectroscopic observations.

During the spring of 2016, the iPTF survey observed the field of iPTF 16abc every night during dark time in either the  $g_{\text{PTF}}$  or  $R_{\text{PTF}}$  band.<sup>2</sup> Survey observations were conducted with the CFH12K camera (Rahmer et al. 2008) on the Palomar Observatory 48-inch telescope (P48; Law et al. 2009). Images were processed by the IPAC image subtraction and discovery pipeline which subtracts off the background galaxy light with stacked pre-SN images and performs forced point-

<sup>2</sup> P48 observations of iPTF 16abc are reported in the  $g_{\text{PTF}}$  and  $R_{\text{PTF}}$  filters throughout, which are similar to the SDSS  $g'$  and Mould- $R$  filters, respectively (see Ofek et al. 2012 for details on PTF calibration). The correction from the  $g_{\text{PTF}}$  and  $R_{\text{PTF}}$  filters to SDSS  $g'$  and  $r'$  requires knowledge of the intrinsic source color (see Eqns. 1 and 2 in Ofek et al. 2012). The spectral diversity of SNe Ia in the days after explosion is poorly constrained, and as a result the color terms for iPTF 16abc at these epochs are unknown. We proceed by assuming the  $g_{\text{PTF}}$  and  $R_{\text{PTF}}$  calibration is on the AB system, which strictly speaking is incorrect, but this does not fundamentally alter any of our conclusions.

spread-function (PSF) photometry at the location of the SN (Masci et al. 2017). The photometry is then calibrated to the PTF photometric catalog (Ofek et al. 2012).

After discovery, photometric observations in the  $g'$ ,  $r'$  and  $i'$  filters were obtained with the SED Machine (SEDm; Blagorodnova et al. 2017, in prep.) mounted on the Palomar Observatory 60-inch telescope (P60). We utilized the Fremling Automated Pipeline (FPipe; Fremling et al. 2016) to subtract galaxy light from the SEDm images using archival Sloan Digital Sky Survey (SDSS) images as a reference. This pipeline then performed forced-PSF photometry at the location of iPTF 16abc, which is calibrated to the SDSS catalog (Ahn et al. 2014).

Photometric observations in the  $BVg'r'i'$  filters were conducted by the Las Cumbres Observatory (LCO) 1-m telescope network. PSF photometry was measured on these images using the `lco_gtsnpipeline` pipeline (Valenti et al. 2016). The  $BV$  magnitudes are calibrated to the Fourth USNO CCD Astrograph Catalog (Zacharias et al. 2013), and the  $g'r'i'$  magnitudes are calibrated to SDSS Data Release 6 (Adelman-McCarthy et al. 2008).

The Reionization and Transients InfraRed (RATIR) camera on the autonomous 1.5 m Harold L. Johnson Telescope at the Observatorio Astronómico Nacional (Butler et al. 2012; Watson et al. 2012) was used to observe iPTF 16abc in the  $r'i'ZYJH$  filters. By design, RATIR lacks a cold shutter, which means IR dark frames are not available. Laboratory testing, however, confirms that the dark current is negligible in both IR detectors (Fox et al. 2012).

The RATIR data were reduced, coadded, and analyzed using standard CCD and IR processing techniques in IDL, Python, SExtractor (Bertin & Arnouts 1996), and SWarp. Aperture photometry is obtained following the methods described in Littlejohns et al. (2014). The  $r'i'Z$  filters are calibrated to SDSS (Ahn et al. 2014), while the  $JH$  filters are calibrated to the Two Micron All Sky Survey (Skrutskie et al. 2006). For the  $Y$ -band calibration, we used an empirical relation in terms of the  $J$  and  $H$  magnitudes derived from the United Kingdom Infrared Telescope (UKIRT; Casali et al. 2007) Wide Field Camera observations (Hodgkin et al. 2009).

The *Swift* satellite observed iPTF 16abc on 14 epochs, beginning  $\sim 15$  d pre-maximum light through  $\sim 22$  d post maximum. The SN flux is measured via aperture photometry on Ultraviolet-Optical Telescope (UVOT) images via the usual procedures in HEASoft, including corrections for coincidence loss and aperture loss. The image counts are converted to physical fluxes using the latest calibration (Breeveld et al. 2011). There are no

pre-SN UVOT images at the SN location in the *Swift* archive. Visual inspection of the UVOT images suggests negligible host-galaxy contamination in our UVOT flux measurements. No X-ray emission is detected from iPTF 16abc by the *Swift* X-ray Telescope (XRT).

The  $g$ -band discovery and follow-up data of iPTF 16abc are illustrated in Figure 1. The photometry is shown in the AB system. As previously noted the color terms necessary to convert  $g_{\text{PTF}}$  to the AB system are unknown and assumed to be zero.

Spectroscopic observations of iPTF 16abc were taken with a variety of telescopes and instruments over multiple epochs spanning from a couple of days after discovery to two months after  $B$ -band maximum. An observing log is listed in Table 1. The spectra were reduced using standard routines in IDL/Python/Matlab. The optical spectral evolution of iPTF 16abc is illustrated in Figure 2, which excludes high-resolution Very Large Telescope (VLT) spectra for clarity.

### 3. HOST GALAXY, REDDENING, AND CLASSIFICATION

#### 3.1. Host Galaxy

The location of iPTF 16abc is spatially coincident with a tidal tail of galaxy NGC 5221. Theureau et al. (2007) derived a distance modulus of  $35.0 \pm 0.4$  mag to NGC 5221 from the Tully-Fisher relation, which is consistent with what we later derive from the SN light curve (see §3.3).

Separately, Courtois & Tully (2015) observe the 21-cm line in NGC 5221 and measure a redshift of 0.0234, which we adopt for the remaining analysis in this paper.

#### 3.2. Reddening

A detailed study of the reddening towards iPTF 16abc is presented in a companion paper (Ferretti et al. 2017, submitted). Briefly, the foreground Galactic extinction toward iPTF 16abc is  $E(B - V) = 0.0279$  mag (Schlafly & Finkbeiner 2011). The high-resolution spectra presented in Ferretti et al. (2017) show multiple absorption components for both the Ca II H+K and Na I D doublets. While the equivalent width (EW) of these lines is quite large, implying a large amount of extinction (e.g., Poznanski et al. 2012), Ferretti et al. compare the evolution of iPTF 16abc to the well-observed normal Type Ia SN 2011fe and find evidence for only a small amount of extinction. The empirical relation between the EW of Na I D and extinction is known to have a large scatter, and Phillips et al. (2013) have shown that Na I D absorption is a poor tracer of reddening in Type Ia SNe. Thus, we instead adopt  $E(B - V) = 0.05$  mag as the local extinction for iPTF 16abc (Ferretti et al. 2017). Thus,

**Table 1.** Spectroscopic observations of iPTF 16abc

Observation	SN			Range
MJD	phase	Telescope	Instrument	(Å)
57483.26	−15.9	DCT	DeVeny <sup>1</sup>	3301–7499
57483.88	−15.3	Gemini-North	GMOS <sup>2</sup>	3800–9200
57484.51	−14.7	Keck-II	DEIMOS <sup>3</sup>	5500–8099
57486.51	−12.7	Keck-II	DEIMOS <sup>3</sup>	5500–8099
57488.38	−10.9	Keck-I	LRIS <sup>4</sup>	3055–10411
57489.51	−9.8	LCO-2m	FLOYDS <sup>5</sup>	3301–8999
57490.40	−8.9	LCO-2m	FLOYDS <sup>5</sup>	3301–9999
57491.55	−7.8	LCO-2m	FLOYDS <sup>5</sup>	3300–9998
57492.20	−7.2	VLT	X-shooter <sup>6</sup>	3300–24550
57494.00	−5.4	VLT	UVES <sup>7</sup>	
57503.32	+3.7	LCO-2m	FLOYDS <sup>5</sup>	3300–9999
57506.00	+6.3	NOT	ALFOSC <sup>8</sup>	3602–8098
57508.27	+8.5	LCO-2m	FLOYDS <sup>5</sup>	3301–9999
57518.42	+18.5	Keck-I	LRIS <sup>4</sup>	3071–10208
57520.03	+20.0	VLT	X-shooter <sup>6</sup>	3300–24789
57529.40	+29.2	LCO-2m	FLOYDS <sup>5</sup>	4000–8998
57542.41	+41.9	LCO-2m	FLOYDS <sup>5</sup>	4000–8998
57550.40	+49.7	LCO-2m	FLOYDS <sup>5</sup>	4001–8999
57562.38	+61.4	LCO-2m	FLOYDS <sup>5</sup>	4800–9300

<sup>1</sup> The Deveny Spectrograph (Bida et al. 2014)

<sup>2</sup> The Gemini Multi-Object Spectrograph (Hook et al. 2004)

<sup>3</sup> DEep Imaging Multi-Object Spectrograph (Faber et al. 2003)

<sup>4</sup> Low-Resolution Imaging Spectrometer (Oke et al. 1995)

<sup>5</sup> FLOYDS <https://lco.global/observatory/instruments/floyds>

<sup>6</sup> X-shooter (Vernet et al. 2011)

<sup>7</sup> Ultraviolet and Visual Echelle Spectrograph (Dekker et al. 2000)

<sup>8</sup> The Andalucia Faint Object Spectrograph and Camera <http://www.not.iac.es/instruments/alfosc>

we assume a total, Galactic + host galaxy, line-of-sight extinction of  $E(B - V) = 0.08$  mag for the remainder of our analysis.

#### 3.3. Classification

Using the SuperNova IDentification (SNID; Blondin & Tonry 2007) package, we find the low-resolution spectrum of iPTF 16abc at +18.8 d is best matched by normal SNe Ia. Several characteristic features of a SN Ia, such as Si II, S II, can be easily identified in the spectra of iPTF 16abc (Figure 2).

To determine the brightness and time of  $B$ -band maximum for iPTF 16abc, we fit the P60 light curves with the

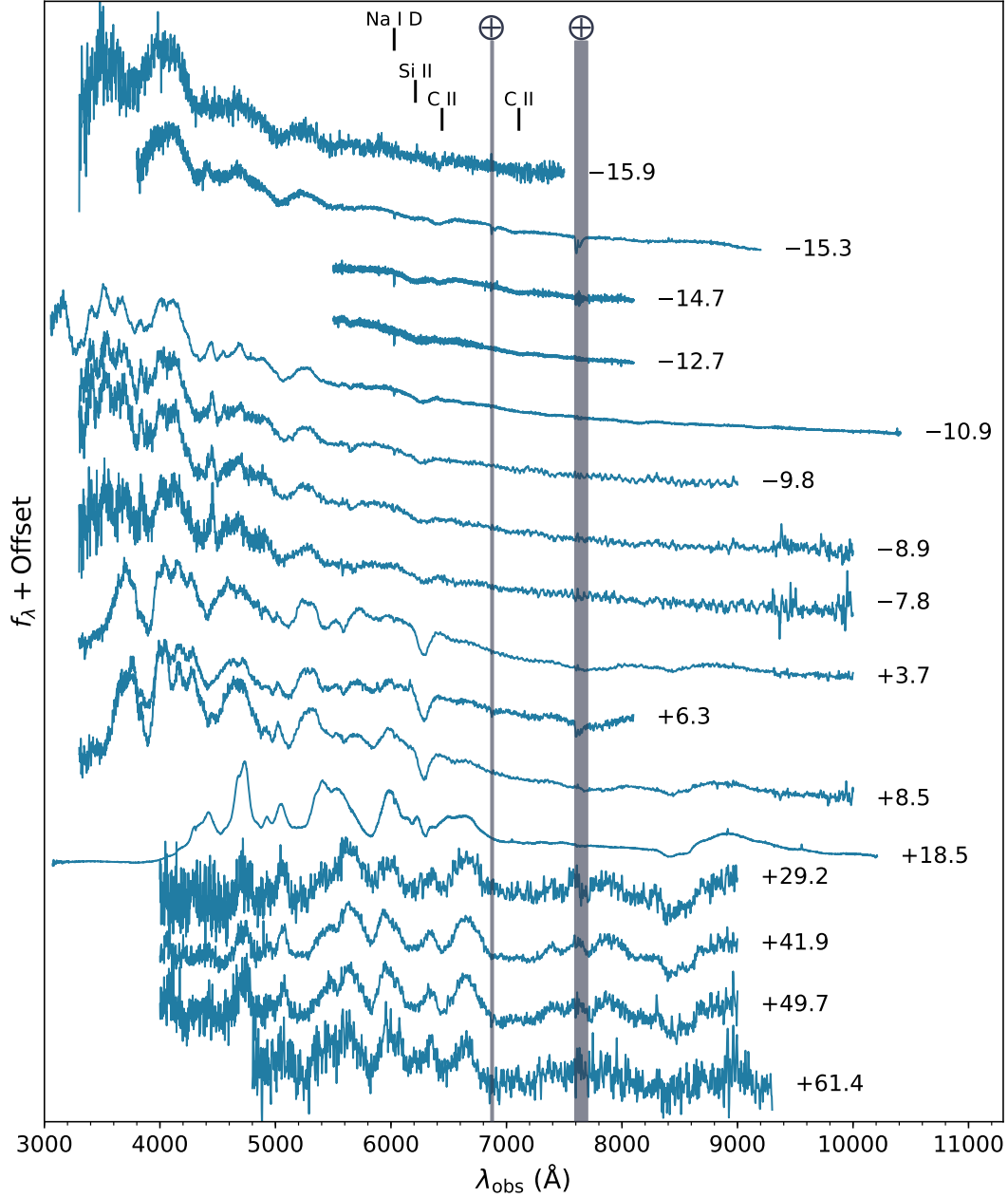


**Figure 2.** Observed spectral sequence of iPTF16abc. The spectra are normalized by their median flux between 6,000 and 7,000 Å. The phase of each spectrum relative to  $T_{B_{\max}}$  is shown. Telluric absorption bands are grayed out. Line identifications are provided for the spectral features discussed in the text. For clarity, high-resolution spectra obtained with the VLT have been omitted (see Ferretti et al. 2017, submitted, for a detailed discussion of these spectra).

`sncosmo` software package.<sup>3</sup> This fit includes a SALT2 template (Guy et al. 2007) that has been corrected for extinction using the (Fitzpatrick 1999) reddening law,  $R_V = 3.1$ , and  $E(B - V) = 0.08$  mag.

We determine the time of rest-frame  $B$ -band maximum to be  $\text{MJD}_{\max} = 57499.54 \pm 0.23$ , the coefficient of

the zeroth principle component  $x_0 = 0.0086 \pm 0.0003$ , the coefficient of the first principle component  $x_1 = 0.96 \pm 0.15$ , and the color term  $c = 0.033 \pm 0.029$ . The best-fit model also gives an unreddened apparent peak magnitude of  $m_B^* = 15.80 \pm 0.04$  mag in the SN rest frame. In the following sections, we define the best-fit value  $\text{MJD}_{\max} = 57499.54$  as the time of  $B$ -band maximum,  $T_{B_{\max}}$ , which we also define as phase  $t = 0$ .

<sup>3</sup> `sncosmo` is available at <https://sncosmo.readthedocs.io>.



We measure the (pseudo)bolometric luminosity,  $L_{UVOIR}$ , of iPTF 16abc at peak via trapezoidal integration of the reddening-corrected flux from the UV, optical, and NIR (UVOIR) filters. The light curves in the individual filters are interpolated so that  $L_{UVOIR}$  is evaluated at common epochs in each filter. From this integration, we determine that iPTF 16abc reaches a maximum luminosity  $L_{\max} = 1.2 \pm 0.1 \times 10^{43} \text{ erg s}^{-1}$ . This value is consistent with the normal SNe Ia studied in Dhawan et al. (2016), a sample which excludes low-luminosity SNe.

After establishing iPTF 16abc as a normal SN Ia, we use the latest calibration (Betoule et al. 2014) of the Phillips relation (Phillips 1993) using  $m_B^*$ ,  $x_1$  and  $c$  to derive a distance modulus  $\mu = 34.89 \pm 0.10 \text{ mag}$  to the SN, provided that the host galaxy of iPTF 16abc has a stellar mass  $< 10^{10} M_{\odot}$ . A more massive host galaxy would result in a larger inferred distance modulus that is nevertheless consistent within the uncertainties. For the following analysis we adopt a distance modulus  $\mu = 34.89 \pm 0.10 \text{ mag}$  for iPTF 16abc.

#### 4. EARLY OBSERVATIONS

Here we consider our suite of early observations of iPTF 16abc, and compare our findings with SN 2011fe, a well-studied, nearby SN that was discovered shortly after explosion (Nugent et al. 2011; Bloom et al. 2012; Piro & Nakar 2014).

##### 4.1. Time of First Light from the Early Light Curve

The time of first light, defined as the moment when appreciable heating from  $^{56}\text{Ni}$  decay has first diffused to the photosphere, for SNe Ia is usually estimated by extrapolating early-phase light curves to determine when the SN flux is equal to 0. Assuming an ideal, expanding fireball with constant temperature, Arnett (1982) derives that  $f \propto t^2$ , where  $f$  is the SN flux and  $t$  is the time since explosion. Despite the basic assumption of a constant temperature at early times, multiple studies have found that the early emission from Type Ia SNe can be described as a power law in time, with power-law index consistent with 2, i.e.  $f \propto t^2$  (e.g., Conley et al. 2006; Hayden et al. 2010b; Ganeshalingam et al. 2011).<sup>4</sup>

As our observations include especially early observations of iPTF 16abc, there are upper limits  $\sim 1 \text{ d}$  prior to the discovery epoch, we model the early flux from iPTF 16abc as a power law, but allow the power-law

index to vary, as opposed to fixing it at 2, to account for potential variations in the photospheric temperature during expansion:

$$f(t) \begin{cases} = 0, & \text{when } t \leq t_0 \\ \propto (t - t_0)^\alpha, & \text{when } t > t_0 \end{cases}, \quad (1)$$

where  $t_0$  is the time of first light,  $\alpha$  is the power-law index, and  $t$  is measured in the SN rest-frame. To determine  $t_0$  and  $\alpha$  we fit the earliest observations of iPTF 16abc. Due to slight variations in the passbands, we fit the model only to the relative flux measured in the  $g_{\text{PTF}}$ -band, which is the only filter with observations prior to first light, a necessity for constraining  $t_0$ .

To determine the best fit parameters, we search a large grid over  $t_0$ ,  $\alpha$ , and the proportionality constant, and minimize  $\chi^2$ . The modeling results show that the SN flux rises approximately linearly between  $t = -18 \text{ d}$  and  $t = -15 \text{ d}$ . Figure 3 shows the best-fit result and the joint marginal distribution of  $t_0$  and  $\alpha$ . From the best-fit model we obtain  $\alpha = 0.98 \pm_{0.14}^{0.16}$  and  $t_0 = -17.91 \pm_{0.15}^{0.07} \text{ d}$ , where the uncertainties represent the marginalized 95% confidence intervals. Our first detection of iPTF 16abc occurred  $\sim 0.15 \text{ d}$  after the SN first light. In the analysis that follows, the precise values of the best-fit parameters are not important. The critical finding here is that  $\alpha \approx 1$  and  $t_0 \approx -18 \text{ d}$ .

As previously noted, a precise determination of the rise time,  $t_{\text{rise}}$ , of SNe Ia is challenging as there may be a “dark phase” following explosion (Piro & Nakar 2014). Nevertheless, to be consistent with previous studies (e.g., Ganeshalingam et al. 2011), here we find  $t_{\text{rise}} = 17.91 \pm_{0.07}^{0.15} \text{ d}$  based on our fit for  $t_0$ . We caution that this measurement may be underestimated due to the uncertain time of explosion.

Simulations presented in Noebauer et al. (2017) show that the flux from SNe Ia explosion models does not evolve as a power law in time. Despite this non-power-law evolution, Noebauer et al. (2017) show that  $f \propto t^\alpha$  models produce good formal fits to simulated observations. The  $f \propto t^\alpha$  fits to the Noebauer et al. models result in glaring errors to the estimated explosion times. Despite the caution advised in Noebauer et al. (2017), we proceed with the power-law fits from above for several reasons. (1) Our primary aim with the fit is to characterize  $\alpha$  for iPTF 16abc compared to SN 2011fe (see below). (2) The errors in the estimated explosion times from Noebauer et al. increase the later the first observation of the SN is obtained. Noebauer et al. only present fits to observations that start  $> 2 \text{ d}$  after explosion, whereas the discovery epoch for iPTF 16abc is likely much earlier than that (see §4.2). (3) We do not

<sup>4</sup> Many of the studies that find  $f \propto t^2$  sample SNe Ia light curves at a phase that is closer to  $T_{B,\max}$  than the initial observations of iPTF 16abc discussed here.

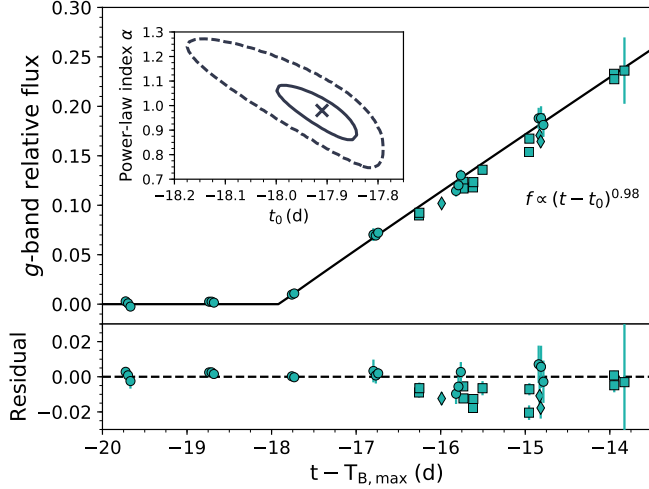


**Figure 3.** Best-fit power-law model to describe the early flux from iPTF 16abc in the  $g_{\text{PTF}}$  band. The model flux, adopting best-fit parameters  $\alpha = 0.98$  and  $t_0 = -17.94$  d, is shown as a solid black line in the top panel. The lower panel shows the model residuals, and the symbols are the same as in Figure 1. The model is fit to just the  $g_{\text{PTF}}$ -band observations to avoid systematic difference between the filters (see the text for further details). The joint distribution of  $t_0$  and  $\alpha$  is illustrated in the inset of the upper panel. The solid and dashed contours represent the 68% and 99.7% confidence levels. [amiller: Update figure to remove other photometry](#)

use the fits to estimate the time of explosion,  $t_0$  instead is an estimate of the time of first light. (4) Pre-discovery upper limits, which are not included in Noebauer et al., provide additional strong constraints on the time of first light. Finally, (5) Noebauer et al. (2017) find that models with strong  $^{56}\text{Ni}$  mixing do follow a power-law evolution, and we explore, and argue in favor of, this possibility for iPTF 16abc (see §5.4).

Unlike iPTF 16abc, the early emission from SN 2011fe is well fit by a  $f \propto t^2$  model (Nugent et al. 2011). Thus, the near-linear rise in flux over the first few days after first light for iPTF 16abc is distinct compared to SN 2011fe. To our knowledge this behavior has only been observed in 2 other SNe (2013dy, 2014J; Zheng et al. 2013, 2014; Goobar et al. 2015). Any model to explain the observations of iPTF 16abc must account for this near-linear rise in the days after first light.

#### 4.2. Time of Explosion from the Photospheric Velocity

The potential dark phase following shock breakout, where SNe Ia are not luminous because the energy deposition from radioactive decay has not had sufficient time to diffuse to the photosphere, means that the explosion time  $t_{\text{exp}} \neq t_0$  in some cases. Piro & Nakar (2014) suggest that measurements of the photospheric velocity

be used to determine  $t_{\text{exp}}$  given that the ejecta begin expanding from the moment of explosion. Assuming a constant opacity in the ejecta, Piro & Nakar find that the photospheric velocity evolves as  $v_{\text{ph}} \propto (t - t_{\text{exp}})^{-0.22}$ . Numerical experiments by Piro & Morozova (2016) find that the constant-opacity assumption strongly depends on the amount of  $^{56}\text{Ni}$  mixing in the SN ejecta (for a more detailed discussion of  $^{56}\text{Ni}$  mixing see §5.4). As a result, the adoption of a  $t^{-0.22}$  power-law model may not be valid for all SNe Ia. Nevertheless, we proceed on the assumption that iPTF 16abc experienced strong  $^{56}\text{Ni}$  mixing, corresponding to the models that are best approximated as a  $t^{-0.22}$  power law. We do this in part to compare with previous studies, though we caution that the inferred value of  $t_{\text{exp}}$  is subject to uncertainties related to ejecta mixing.

While the photospheric velocity is not easy to measure, line velocities of Si II or Ca II can be used as a proxy (Piro & Nakar 2014; Shappee et al. 2016b). In the case of iPTF 16abc, the Ca II IR triplet is very weak, likely due to high temperatures in the ejecta. Thus, we determine the photospheric velocity from the Si II  $\lambda 6355$  line. Visual inspection shows no sign of multi-velocity components of Si II, and that the C II  $\lambda 6580$  line overlaps the red wing of the Si II line (see Figures 2 and 5). Consequently, we model the observed spectra between 5,900 and 6,500 Å (rest-frame) as the combination of two Gaussian kernels plus a linear baseline, which accounts for Si II, C II and the continuum, respectively. The expansion velocity of Si II is measured by the central wavelength of the Si II Gaussian kernel.

We fit the measured velocities of Si II  $\lambda 6355$  to the  $v \propto (t - t_{\text{exp}})^{-0.22}$  model by minimizing the  $\chi^2$  value and find the best-fit explosion time relative to  $T_{\text{B,max}}$  in the SN rest frame to be  $t_{\text{exp}} = -17.45 \pm_{0.16}^{0.14}$  d, where the uncertainties represent the 95% confidence interval (Figure 4). Following the analysis in Piro & Nakar (2014), we additionally alter the power-law index to  $-0.20$  and  $-0.24$  to examine the sensitivity of the result on the assumed power-law index. We find that this variation in the power-law index results in inferred explosion times that vary by  $\approx 1$  d (Figure 4). Given the analytical approximation that  $v \propto t^{-0.22}$ , we adopt  $t_{\text{exp}} = -17.5 \pm 0.5$  d, where the uncertainty reflects possible variations in the power-law index (see Piro & Nakar 2014).

Comparing our estimates for  $t_{\text{exp}}$  and  $t_0$  (left panel of Figure 4), we find that  $t_0 \lesssim t_{\text{exp}}$ . Since physical causality requires  $t_{\text{exp}} \leq t_0$ , we draw the qualitative conclusion that  $t_0 \simeq t_{\text{exp}}$ , which is consistent to within the uncertainties. Again, we caution that this derivation of  $t_{\text{exp}}$  relies on the assumption  $v \propto t^{-0.22}$ , which may not be valid for all SNe Ia.



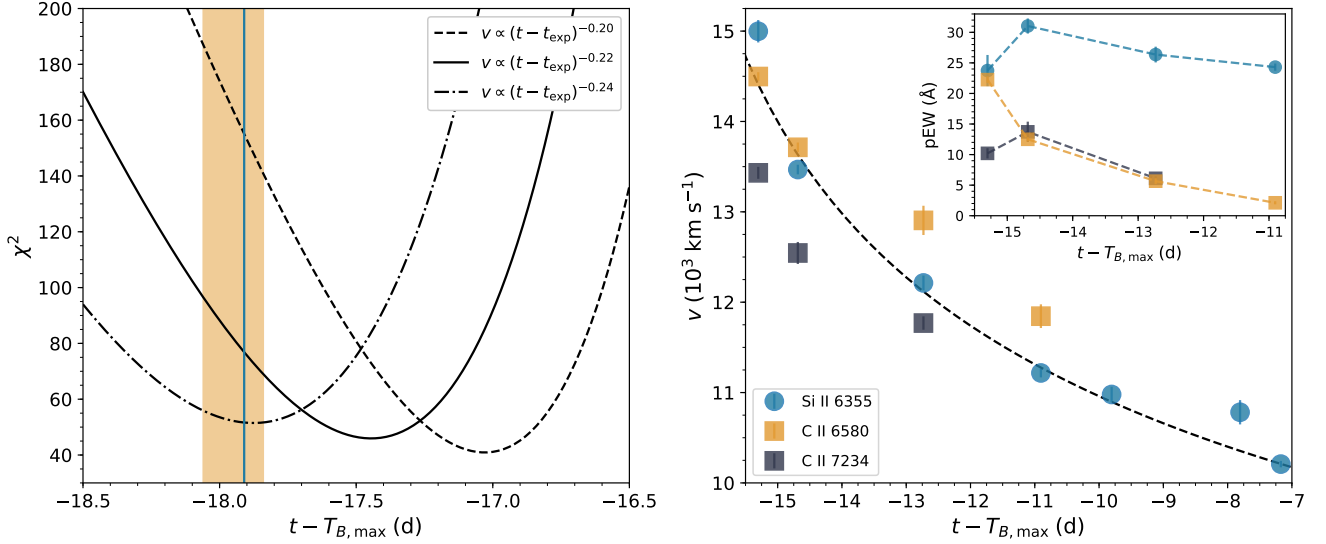


**Figure 4.** Constraints on  $t_{\text{exp}}$  from fitting the velocity evolution of Si II. *Left panel:* the dashed, solid and dash-dotted curves show  $\chi^2$  for fitting power laws with indices  $-0.20$ ,  $-0.22$  and  $-0.24$ , respectively. The blue vertical line and the orange shaded region indicate  $t_0$  and its 95% confidence interval from Section 4.1, respectively. *Right panel:* Observed Si II  $\lambda 6355$  velocities (blue circles) and the best-fit power-law model with an index of  $-0.22$  (dashed line). Additionally, the measured velocities of C II  $\lambda\lambda 6580$ , 7234 are shown. Typical uncertainties are smaller than the size of the points. *Right inset:* Evolution of the pseudo-equivalent width of Si II  $\lambda 6355$ , and C II  $\lambda\lambda 6580$ , 7234 in the  $\sim 7$  d following explosion.

#### 4.3. Strong and Short-Lived Carbon Features

The early spectra of iPTF 16abc exhibit unusually strong absorption due to C II  $\lambda\lambda 6580$ , 7234. We highlight the evolution of these spectral features in Figure 5. From these spectra we see that C II  $\lambda 6580$  is as strong as Si II  $\lambda 6355$  at  $t \approx -15$  d. The strength of the C II lines declines with time, and by  $t \approx -10$  d C II is no longer detectable.

Similar to our analysis of the Si II  $\lambda 6355$  line, we can measure velocities and pseudo-equivalent widths (pEWs) of C II  $\lambda\lambda 6580$ , 7234. We compare the velocity evolution of the C II lines to Si II in the right panel of Figure 4, which also shows the pEW evolution of these lines. These measurements confirm the qualitative analysis from Figure 5: namely, the pEW of C II  $\lambda 6580$  is comparable to that of Si II  $\lambda 6355$  at  $t \approx -16$  d and the pEW of C II decreases until the feature is no longer detectable around  $t = -10$  d.

The detection of C II in SNe Ia spectra is relatively rare as it requires both unburned carbon, which is likely only present in the outermost layers of the ejecta, and non-local thermal equilibrium effects in order to excite the ionized carbon (e.g., Thomas et al. 2007). Spectra obtained around or after  $T_{B,\text{max}}$  rarely show C II as the photosphere has receded from the outermost ejecta, while pre-max spectra show evidence for C II in  $\sim 1/4$  of all normal SNe Ia (e.g., Parrent et al. 2011; Silverman & Filippenko 2012; Thomas et al. 2011), but the signatures are typically weak. While we caution that the

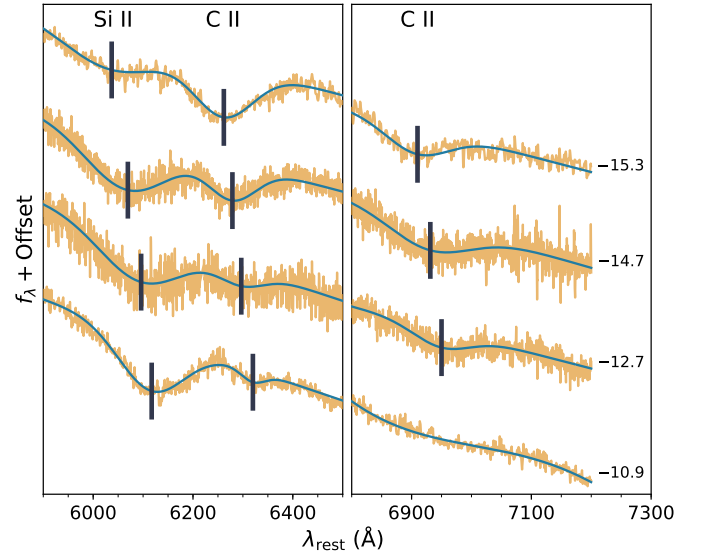


**Figure 5.** Evolution of the C II features observed in the early spectra of iPTF 16abc. The raw spectra are shown in orange, while the solid blue lines show the best-fit models including Gaussian components for each line and a linear component for the continuum (see text for further details). The dark grey vertical lines show the measured line centers, indicating the decline in the photosphere velocity in the  $\sim 7$  d after explosion (note that C II  $\lambda 7234$  is not detected in the  $-10.9$  d spectrum). The phase of each spectrum relative to  $T_{B,\text{max}}$  is labeled.

sample of SNe Ia with spectra taken within a few days of explosion is small, SNe 2013dy and 2017cbv are the

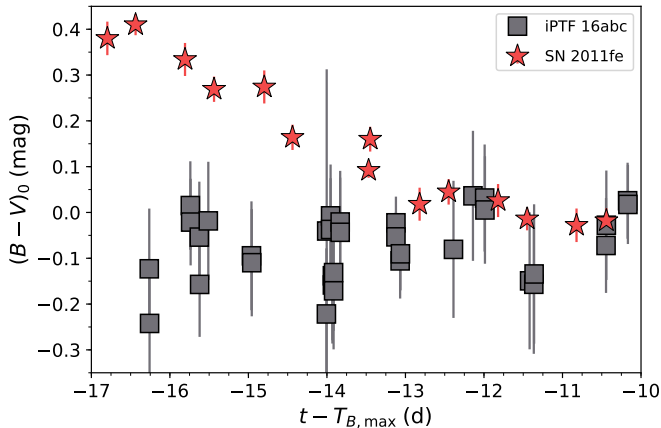


**Figure 6.**  $(B - V)_0$  color evolution of iPTF 16abc (shown as squares) compared to SN 2011fe (shown as stars). The  $B$  and  $V$  photometry are calibrated on the Vega system, and have been corrected for extinction. The data for SN 2011fe are from Zhang et al. (2016).

only other objects known to have strong C II features like iPTF 16abc (Zheng et al. 2013; Hosseinzadeh et al. 2017). As a counterexample, SN 2011fe only exhibited weak C II features in its first spectra (Parrent et al. 2012). Thus, models of iPTF 16abc must explain the strong C II absorption observed shortly after explosion.

#### 4.4. Blue Optical Colors Shortly After Explosion

Multiband observations of iPTF 16abc began  $\sim 1.5$  d after discovery, which allows us to trace its color evolution starting  $\sim 1.7$  d after  $t_0$ . In Figure 6 we compare the  $(B - V)_0$  color evolution of iPTF 16abc and SN 2011fe, where the observations of SN 2011fe are taken from Zhang et al. (2016). For both SNe the colors have been corrected for the total inferred reddening along the line of sight. Interestingly, iPTF 16abc has a nearly flat color evolution up to 10 d before  $T_{B,\max}$ , while SN 2011fe exhibits red colors initially before evolving to the blue.

Roughly 16 d prior to  $B$ -band maximum, the  $(B - V)_0$  color of iPTF 16abc is  $\sim 0.5$  mag bluer than SN 2011fe. Like iPTF 16abc, SN 2012cg (Marion et al. 2016) and SN 2017cbv (Hosseinzadeh et al. 2017) exhibit  $(B - V)_0$  colors that are significantly bluer than SN 2011fe at very early epochs. While there are many factors that contribute to the early optical colors of SNe Ia (see §5 below), early blue colors are often interpreted as a hallmark of interaction between the SN ejecta and a binary companion. Nevertheless, it is interesting to note that despite the blue optical colors, the UV – optical colors of iPTF 16abc, SN 2012cg, and SN 2017cbv are significantly redder at these early epochs than the UV – optical colors of iPTF 14atg (Cao et al. 2015), the most likely candidate for SN ejecta-companion interaction.

## 5. DISCUSSION

Relative to the nearby, normal SN 2011fe, we have identified several distinct characteristics of the early evolution of iPTF 16abc, including: (i) a near-linear photometric rise, (ii) a qualitatively short dark phase, assuming  $v_{\text{ph}} \propto t^{-0.22}$ , (iii) the presence of strong C II absorption, and (iv) blue and non-evolving  $(B - V)_0$  color in the week after explosion. While most SNe Ia are powered purely by radioactive decay, the observed radiation shortly after explosion can also include contributions from SN shock cooling or the collision of the SN ejecta with a non-degenerate companion or diffuse material. Here we consider those scenarios as a possible explanation for the early behavior of iPTF 16abc.

### 5.1. SN Shock Cooling

The shock breakout of a SN Ia lasts for a fraction of a second due to compact size of the exploding star. Emission from the subsequent cooling phase may last for several days, however (e.g., Piro et al. 2010). Following the analysis of Bloom et al. (2012) for SN 2011fe, we compare the early-phase  $g_{\text{PTF}}$  light curve of iPTF 16abc with two shock cooling models (Rabinak & Waxman 2011; Piro et al. 2010). From this analysis, we constrain the iPTF 16abc progenitor radius to be  $< 1 R_{\odot}$ . Our observations of iPTF 16abc cannot place tight constraints on the size of SN Ia progenitors. Indeed, for a typical WD radius, such as that inferred for SN 2011fe ( $\lesssim 0.02\text{--}0.04 R_{\odot}$ ; Bloom et al. 2012; Piro & Nakar 2014), the expected emission from shock cooling is  $\sim 2$  mag fainter than the P48  $g_{\text{PTF}}$  detection limit at this distance. Thus, we conclude that shock cooling does not contribute to the early emission from iPTF 16abc.

### 5.2. SN-Companion collision

The detection of excess emission due to the collision of the SN ejecta with a non-degenerate companion requires a favorable orbital alignment relative to the line of sight. Thus, from geometric considerations alone the probability of detecting ejecta-companion interaction is low,  $\sim 10\%$ . Kasen (2010) calculates that the collision of SN ejecta with a companion generates thermal emission with a spectrum that peaks in the UV. The resulting  $g$ -band emission is expected to be weak.

To examine the possibility of a SN-companion signature in the early light curve of iPTF 16abc, we employ the Kasen (2010) model and assume canonical values for the ejecta mass,  $1.4 M_{\odot}$ , expansion velocity,  $10^4 \text{ km s}^{-1}$ , and a constant opacity,  $0.2 \text{ cm}^2 \text{ g}^{-1}$ . We calculate the expected  $g_{\text{PTF}}$  brightness of an ejecta-companion collision at the distance of iPTF 16abc behind a total reddening of  $E(B - V) = 0.08 \text{ mag}$  using the parameterized

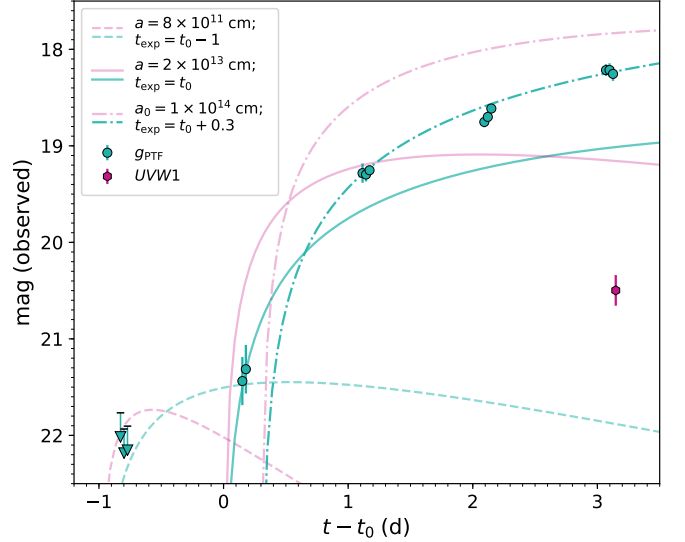
equations in Brown et al. (2012). If we assume the binary is aligned with the optimal orientation relative to the line of sight, a binary separation of  $a \approx 2 \times 10^{13}$  cm is needed to explain the initial detection of iPTF 16abc, as shown in Figure 7. This model does not, however, match the  $g_{\text{PTF}}$  evolution for  $t > t_0 + 1$  d (though it is possible that the SN photosphere dominates the companion-interaction signature at this phase). Furthermore, this model significantly overpredicts the observed flux in the *Swift*/UVW1 filter  $\sim 3.1$  d after  $t_0$ . As such, we do not favor such a model as the explanation for the early emission from iPTF 16abc.

Figure 7 additionally shows that a companion at  $a = 10^{14}$  cm provides a good match to the observations  $\sim 1$ – $3$  d after  $t_0$  if  $t_{\text{exp}} \approx t_0 + 0.3$  d. Like the  $a = 2 \times 10^{13}$  cm model, this model significantly overpredicts the observed UV flux from iPTF 16abc. Additionally, this model cannot account for the brightness of iPTF 16abc at the epoch of discovery. The challenges associated with each of the previous two models lead us to conclude that the early evolution of iPTF 16abc cannot be explained via the interaction of the SN ejecta with a red-giant companion.<sup>5</sup> We cannot, however, exclude the presence of a red-giant companion as our calculations have assumed that the binary is aligned with the optimal geometry relative to the line of sight. If the geometry is not favorable, then it is possible that signatures from interaction with a companion are not visible.

Finally, we examine the minimum binary separation capable of explaining the observed brightness at the epoch of discovery. Figure 7 shows that models with  $a \approx 8 \times 10^{11}$  cm peak at  $\sim 21.5$  mag in the  $g_{\text{PTF}}$ -band, provided that  $t_{\text{exp}} \approx t_0 - 1$  d. To explain just the epoch of discovery, models with larger  $a$  would require even earlier explosion times, which is not compatible with our non-detections the night before discovery, while models with smaller  $a$  are not bright enough. While it is otherwise compatible with the observations, we do not favor the  $a \approx 8 \times 10^{11}$  cm model as the explanation for the early flux from iPTF 16abc because it does not explain the 2 mag rise in the  $\sim 24$  hr after discovery.

### 5.3. Interaction with Diffuse Material

To model SN 2011fe, Dessart et al. (2014) recently examined pulsational delayed-detonation (PDD) models as an explanation for some SNe Ia. Briefly, PDD models differ from “standard” delayed detonation (DD) models in that the initial deflagration causes the WD to expand resulting in the release of some unbound material. As



**Figure 7.** Comparison of SN ejecta-companion interaction models with early observations of iPTF 16abc.  $g_{\text{PTF}}$  observations (green) detections and  $3\sigma$  upper limits are shown as circles and downward arrows, respectively. The initial *Swift*/UVW1 observation (magenta) is shown as a hexagon. The dashed, solid, and dash-dot lines show the expected flux for various companion interaction models in the  $g_{\text{PTF}}$  (green) and UVW1 (magenta) filters. The models have been adjusted to account for the distance and reddening towards iPTF 16abc. Each model features a different companion semi-major axis,  $a$ , and time of explosion,  $t_{\text{exp}}$ , as labeled in the legend. While models with  $a \gtrsim 10^{13}$  cm can explain the early  $g_{\text{PTF}}$  emission, they greatly overpredict the flux in the UV. If the time of explosion is  $\sim 1$  d prior to  $t_0$ , then models with  $a \approx 10^{12}$  cm can explain the initial detection iPTF 16abc, but they fail to replicate the  $\sim 2$  mag rise in the  $\sim 24$  hr after explosion.

the bound material contracts, eventually a subsequent detonation occurs.<sup>6</sup> An important consequence of this progression for PDD models is that they naturally produce material that avoids burning, unlike DD models that typically leave no unburnt material. This results in significantly more carbon in the outer layers of the SN ejecta (Dessart et al. 2014).

When comparing observations of SN 2011fe to their DD models, Dessart et al. (2014) find that the models are universally too faint and red at early times,  $\sim 24$ – $48$  hr after explosion. Instead, Dessart et al. (2014) find that PDD models provide a better match to observations. Briefly, the diffuse material surrounding the WD heats the outer layers of the SN ejecta leading to a steeper more luminous rise, with bluer colors in the few days after explosion. Importantly, the PDD mod-

<sup>5</sup> The Kasen (2010) model assumes Roche-lobe overflow, meaning that  $a > 10^{13}$  cm implies a companion with  $R_* \gtrsim 100 R_{\odot}$ .

<sup>6</sup> Dessart et al. (2014) note that the deflagration and detonation in their PDD models are artificially triggered.

els are nearly indistinguishable from DD models around and post peak.

Qualitatively, the PDD models provide a better match to the observations of iPTF 16abc than DD models. In particular, PDD models provide higher luminosities and faster rise times in the days after explosion, a more rapid evolution towards blue optical colors, and the formation of strong C II lines that gradually disappear in the  $\sim$ week after explosion. Quantitatively, there are still some shortcomings of the models presented in Dessart et al. (2014). In particular, the power-law index for the  $g$ -band rise is  $\alpha \approx 3$  for each of the PDD models, which is significantly more steep than  $\alpha = 0.98$ , which we measure for iPTF 16abc. The optical colors for iPTF 16abc are blue from our first epoch  $\sim 1.7$  d after explosion and remain approximately constant in the 10 d after explosion, whereas the PDD models in Dessart et al. (2014) either exhibit distinct color evolution (i.e. are not constant) or are too red in the first few days after explosion. Nevertheless, the PDD models presented in Dessart et al. (2014) provide several attractive explanations for the unusual features in the early behavior of iPTF 16abc, and it may be possible that small adjustments to the model (e.g., additional mixing of the radioactive material, adjustments in the explosion energy, etc.) can better match iPTF 16abc.

#### 5.4. Strong $^{56}\text{Ni}$ Mixing in the SN Ejecta

Having examined other possibilities we now consider whether the unusual properties of iPTF 16abc can be explained simply by invoking strong mixing in the SN ejecta. Strong mixing can lead to a short dark phase. Here we additionally examine whether strong mixing can explain the rapid, near-linear rise in the light curve.

In Figure 8 we compare model calculations from Piro & Morozova (2016) to the observed photometry of iPTF 16abc. The Piro & Morozova models employ a piston driven explosion to explode a single WD progenitor model. As the piston explosion does not result in any nucleosynthesis, the distribution of  $^{56}\text{Ni}$  in the ejecta must be prescribed by hand, which enables a study of the effects of mixing on the resulting SN emission. Each model employs a fixed  $0.5 M_{\odot}$  of  $^{56}\text{Ni}$  that has been distributed throughout the ejecta via boxcar averaging (see their Figure 1). The resulting light curves are synthesized using the SuperNova Explosion Code (SNEC; Morozova et al. 2015), as shown in Figure 8. Broadly speaking, the results can be summarized as follows: SN with strong mixing exhibit a rapid almost linear rise and quickly develop blue colors, whereas models where the  $^{56}\text{Ni}$  is confined to the innermost layers of the ejecta remain very faint for days after explosion while exhibit-

ing relatively red optical colors during this period. The fast rise and blue color of iPTF 16abc are qualitatively consistent with the strong mixing models from Piro & Morozova (2016), as shown in Figure 8. In fact, if we adopt  $t_{\text{exp}} = t_0 - 0.4$  d, we find that the model with the strongest mixing (orange line in Figure 8) provides an excellent match to the  $g$ -band observations.

While the models from Piro & Morozova (2016) provide a good match to the optical photometric evolution of iPTF 16abc, they consistently overpredict the flux in the UV. The models shown in Figure 8 also overpredict the photospheric velocity of iPTF 16abc by  $\sim 2$ – $3,000 \text{ km s}^{-1}$ . These discrepancies may be accounted for following an improved treatment of line-blanketing and a reduction in the model explosion energy, respectively. Future modeling efforts may improve the match between the simulations and observations for iPTF 16abc.

Both the PDD models and ejecta-mixing models show discrepancies with some early observations of iPTF 16abc. Nevertheless, we conclude that one, or both, of these scenarios, which feature qualitatively similar predictions, is the most likely explanation for iPTF 16abc. Indeed, it may be the case that the typical sequence of photometric and spectroscopic observations of young SNe Ia can never distinguish between these two possibilities (Noebauer et al. 2017).

#### 5.5. The Emerging Sample of Young SNe Ia

The proliferation of high-cadence, time-domain surveys has led to several SNe Ia being discovered within  $\lesssim 2$  d of first light in the past  $\sim$ decade. Observations probing the early evolution of these SNe allows us to place unique constraints on their progenitor systems and the corresponding explosion physics. This has revealed diversity in the earliest epochs after explosion and that commonly used SNe Ia templates do not match observations (e.g., Foley et al. 2012).

In §4 we compared our early observations of iPTF 16abc to SN 2011fe, which has the most comprehensive observations of the young SNe Ia sample. Given its normal spectroscopic and photometric evolution, SN 2011fe has been adopted as a standard for the early evolution of SNe Ia in many studies. While a detailed quantitative analysis is beyond the scope of this study, a qualitative examination of very young SNe Ia that otherwise exhibit normal spectra and evolution at and post-peak<sup>7</sup> reveals considerable diversity. In other words, at early times SN 2011fe may not be the norm.

<sup>7</sup> This definition excludes iPTF 14atg, which was shown to be subluminal with SN 2002es-like spectra (Cao et al. 2015).



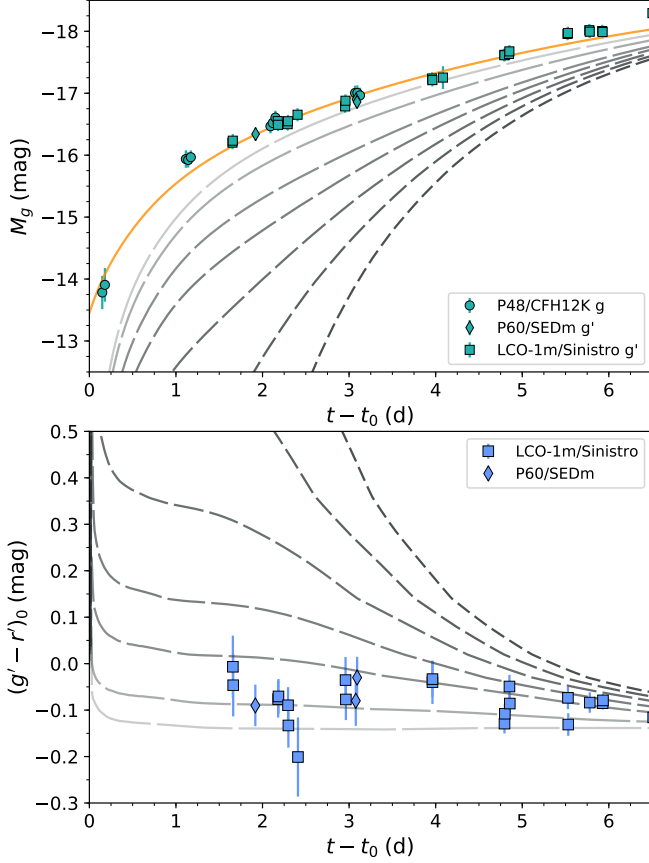


**Figure 8.** Photometric comparison of iPTF 16abc and the theoretical models of Piro & Morozova (2016). The amount of  $^{56}\text{Ni}$  mixing in the SN ejecta increases from the short-dash, dark lines to the long-dash, light lines. *Top:*  $M_g$  vs. time, where the observed  $g$ -band magnitudes have been corrected to  $M_g$  using the distance modulus to iPTF 16abc (§3.1) and the total line-of-sight reddening ( $E(B - V) = 0.08$  mag; Ferretti et al. 2017, submitted). The orange solid line shows the model with the most  $^{56}\text{Ni}$  mixing shifted to an explosion time of  $t_0 - 0.4$  d. This model provides a good match to the data. *Bottom:*  $(g' - r')_0$  vs. time. The observed colors have been corrected for reddening.

For SN 2011fe the initial rise is well described by a  $t^2$  power law, the  $(B - V)_0$  colors evolve from the red to the blue in the  $\sim$ week after explosion, and the C II present in the initial spectra is weak (Nugent et al. 2011; Zhang et al. 2016; Parrent et al. 2012). In contrast, iPTF 16abc exhibits a near linear rise in flux, the  $(B - V)_0$  colors are blue and roughly constant, and the C II absorption is strong. Examining just these 3 qualitative features, SN 2009ig is well matched to SN 2011fe (Foley et al. 2012), while SN 2013dy (Zheng et al. 2013), SN 2017cbv (Hosseinizadeh et al. 2017), and iPTF 16abc all bear a striking resemblance. SN 2012cg, on the other hand, is intermediate to these two groups with weak C II and a relatively shallow early rise, like SN 2011fe, but

blue  $(B - V)_0$  colors, like iPTF 16abc (Silverman et al. 2012; Marion et al. 2016). SN 2014J is intermediate in the other direction in that it exhibits a near linear rise (Zheng et al. 2014; Goobar et al. 2015), but the color evolution is very similar to SN 2011fe (Amanullah et al. 2014).<sup>8</sup> That these early observations cannot be easily separated into two distinct groups suggests that it is unlikely that a single physical mechanism drives the diversity of SNe Ia at early times.

In the case of SN 2012cg and SN 2017cbv it has been argued that the early blue optical colors are indicative of interaction between the SN ejecta and a binary companion (Marion et al. 2016; Hosseinizadeh et al. 2017). SN 2017cbv is particularly remarkable in that the observations presented in Hosseinizadeh et al. (2017) show a clearly resolved bump in the  $U$ ,  $B$ , and  $g'$  bands in the  $\sim 5$  d after explosion. In Hosseinizadeh et al. it is found that the bump can be explained via the combination of ejecta-companion interaction and the normal evolution of a SN Ia. A challenge for this model, similar to iPTF 16abc (see §5.2), is that it significantly overpredicts the UV brightness of the SN compared to what is observed. Indeed, in the case of SNe 2012cg, 2017cbv, and iPTF 16abc the UV – optical colors are significantly redder than those observed in iPTF 14atg. It is argued in Hosseinizadeh et al. (2017) that several model assumptions, including: (i) ideal blackbody emission, (ii) a constant opacity, (iii) a simple power-law density profile for the ejecta, and (iv) spherical symmetry, may be incorrect, which could reconcile the discrepancy with the UV observations. Above, we argued for circumstellar interaction and strong  $^{56}\text{Ni}$  mixing as a possible explanation for iPTF 16abc, and indeed Hosseinizadeh et al. (2017) consider these possibilities for SN 2017cbv as well. Separately, several arguments against companion interaction for SN 2012cg are presented in Shappee et al. (2016a).

Ultimately, there are arguments in favor of and against each of the possibilities to explain the early emission from SNe Ia. Moving forward, more detailed models and simulations are needed to properly explain the observed diversity. No matter the correct explanation for the early behavior of SNe 2013dy, 2017cbv, and iPTF 16abc, the strong similarities between these events suggests that they may reflect a common physical origin.

<sup>8</sup> C II is not detected in the spectra of SN 2014J (Goobar et al. 2014; Zheng et al. 2014), though the earliest spectra of SN 2014J were obtained at a much later phase than the other SNe discussed here. Marion et al. (2015) find evidence for C I in the NIR spectra of SN 2014J, but this detection cannot constrain the relative strength of C II and Si II shortly after explosion.



## 6. CONCLUSION

We have presented observations of the extraordinarily early discovery of the normal Type Ia supernova iPTF 16abc. Our fast-response follow-up campaign allowed us to draw the following conclusions:

- Extrapolation of the early light curve shows that the initial detection of iPTF 16abc occurred only  $0.15 \pm_{0.07}^{0.15}$  d after the time of first light,  $t_0$ .
- We find no evidence for detectable signatures of SN shock cooling or the collision of the SN ejecta with a non-degenerate binary companion.
- Assuming that  $v_{\text{ph}} \propto t^{-0.22}$ , then  $t_{\text{exp}} \approx t_0$ . A short dark phase, as this implies, is likely the result of either strong  $^{56}\text{Ni}$  mixing or interaction of the SN ejecta with diffuse material.
- The strong and short-lived carbon features seen in the earliest spectra of iPTF 16abc can only be explained if there is incomplete burning. The pulsational delayed detonation models presented in Dessart et al. (2014) produce C II absorption that is as strong as Si II at very early phases.
- In contrast to SN 2011fe,  $(B - V)_0$  is  $\sim 0.5$  mag bluer for iPTF 16abc  $\sim 2$  d after  $t_0$ . Furthermore, the  $(B - V)_0$  colors of iPTF 16abc show no evolution over the first  $\sim 7$  d of observations.
- Finally, we show that the early light curve evolution and colors of iPTF 16abc are well matched by the theoretical models of Piro & Morozova (2016) that include significant mixing of  $^{56}\text{Ni}$  into the outer layers of the SN ejecta.

Taken together, these observations all indicate that the nucleosynthetic products from the explosion are well mixed throughout the SN ejecta. There are elements of the PDD models from Dessart et al. (2014) that are attractive for explaining iPTF 16abc, in particular, the strong C II absorption seen at early times. In the future, it would be useful to investigate more detailed PDD models that incorporate strong  $^{56}\text{Ni}$  mixing to see if they better replicate the observations of iPTF 16abc as it is otherwise difficult to distinguish between these two scenarios (Noebauer et al. 2017).<sup>9</sup>

Extremely early observations of young SNe provide a “smoking gun” to probe the mixing level in the ejecta,

which, in turn, is a result of the explosion mechanism. Wide-field, high-cadence surveys, such as the Zwicky Transient Facility (Bellm 2016) and ATLAS (Tonry 2011, 2013), will discover a large number of very young SNe over the next few years, allowing us to extend our studies beyond single objects. While the sample of extremely young SNe Ia will grow by more than an order of magnitude, the detection of shock breakout cooling and ejecta-companion interaction will prove challenging. Given the diminutive size of WDs, the thermal emission following shock breakout can only be detected to  $\sim 10$  Mpc on 1-m class telescopes. Furthermore, only  $\sim 10\%$  of single-degenerate progenitors are expected to give rise to detectable emission following the collision of the SN ejecta with the binary companion (Kasen 2010). Despite these limitations, this study of iPTF 16abc shows that the early detection of SNe Ia can probe explosion physics by measuring the amount of mixing in the SN ejecta. Moving forward, a large sample of such objects will enable strict constraints on the proposed explosion mechanisms for Type Ia SNe.

Finally, we close by emphasizing the importance of fast-response photometric and spectroscopic follow-up campaigns. Without the early recognition of the youth of this SN, and the associated follow-up, much of the analysis presented herein would not have been possible. The ability to trigger such observations is essential to improve our understanding of the physics of SNe Ia.

We are deeply grateful to R. C. Thomas for indulging a slew of questions regarding C II in SNe. Similarly, it is our pleasure to buy a beer for R. Amanullah and U. Feindt for discussions regarding SALT2.

This paper utilizes the LCO infrastructure for rapid and regular monitoring of SNe, and we thank S. Valenti and I. Arcavi for their development efforts.

Much of the analysis presented herein would not have been possible without the help of several observers. We thank M. West for taking the first spectrum of iPTF 16abc as a ToO on the DCT. We also thank P. GuhaThakurta, E. C. Cunningham, K. A. Plant, H. Jang, and J. Torres for executing a Keck ToO as part of the UC/Caltech partnership, and also the Gemini service observers for executing our ToO observations. Additionally, J. Cohen, N. Suzuki, V. Ravi, R. Walters, A. Ho, H. Vedantham, K. De, and L. Yan helped obtain data for this paper.

AAM is funded by the Large Synoptic Survey Telescope Corporation in support of the Data Science Fellowship Program. YC thanks support from a postdoc fellowship in the eScience institute, University of Washington.

<sup>9</sup> Both Dessart et al. (2014) and Piro & Morozova (2016) consider models with strong mixing *and* interaction, but those studies do not replicate each of the salient features of iPTF 16abc.

DAH, CM, and GH are supported by NSF-1313484.

The Intermediate Palomar Transient Factory project is a scientific collaboration among the California Institute of Technology, Los Alamos National Laboratory, the University of Wisconsin, Milwaukee, the Oskar Klein Center, the Weizmann Institute of Science, the TANGO Program of the University System of Taiwan, and the Kavli Institute for the Physics and Mathematics of the Universe. This work was supported by the GROWTH project funded by the National Science Foundation under Grant No 1545949. Part of this research was carried out at the Jet Propulsion Laboratory, California Institute of Technology, under a contract with the NASA. This work makes use of observations from the LCO net-

work. These results made use of the Discovery Channel Telescope at Lowell Observatory. Lowell is a private, non-profit institution dedicated to astrophysical research and public appreciation of astronomy and operates the DCT in partnership with Boston University, the University of Maryland, the University of Toledo, Northern Arizona University and Yale University. The upgrade of the DeVeny optical spectrograph has been funded by a generous grant from John and Ginger Giovale.

*Facility:* DCT, Gemini:Gillett, Hale, Keck:I, Keck:II, LCOGT, PO:1.2 m, PO:1.5 m, VLT, Swift, OANSPM:HJT

*Software:* PTFIDE (Masci et al. 2017), FPIPE, SALT2, SNID, lcogtsnpipe, UVOTSOURCE.

## APPENDIX

### A. PHOTOMETRIC LIGHT CURVES

The full photometric light curves of iPTF 16abc are shown in Figure 9.

## REFERENCES

- Adelman-McCarthy, J. K., Agüeros, M. A., Allam, S. S., et al. 2008, *ApJS*, 175, 297
- Ahn, C. P., Alexandroff, R., Allende Prieto, C., et al. 2014, *ApJS*, 211, 17
- Amanullah, R., Goobar, A., Johansson, J., et al. 2014, *ApJL*, 788, L21
- Arnett, W. D. 1982, *ApJ*, 253, 785
- Bellm, E. C. 2016, *PASP*, 128, 084501
- Bertin, E., & Arnouts, S. 1996, *A&AS*, 117, 393
- Betoule, M., Kessler, R., Guy, J., et al. 2014, *A&A*, 568, A22
- Bianco, F. B., Howell, D. A., Sullivan, M., et al. 2011, *ApJ*, 741, 20
- Bida, T. A., Dunham, E. W., Massey, P., & Roe, H. G. 2014, in *Proc. SPIE*, Vol. 9147, Ground-based and Airborne Instrumentation for Astronomy V, 91472N
- Blondin, S., & Tonry, J. L. 2007, *ApJ*, 666, 1024
- Bloom, J. S., Kasen, D., Shen, K. J., et al. 2012, *ApJL*, 744, L17
- Breeveld, A. A., Landsman, W., Holland, S. T., et al. 2011, in *American Institute of Physics Conference Series*, Vol. 1358, American Institute of Physics Conference Series, ed. J. E. McEnery, J. L. Racusin, & N. Gehrels, 373–376
- Brown, P. J., Dawson, K. S., Harris, D. W., et al. 2012, *ApJ*, 749, 18
- Butler, N., Klein, C., Fox, O., et al. 2012, in *Proc. SPIE*, Vol. 8446, Ground-based and Airborne Instrumentation for Astronomy IV, 844610
- Cao, Y., Kulkarni, S. R., Howell, D. A., et al. 2015, *Nature*, 521, 328
- Casali, M., Adamson, A., Alves de Oliveira, C., et al. 2007, *A&A*, 467, 777
- Cenko, S. B., Cao, Y., Kasliwal, M., et al. 2016, *The Astronomer’s Telegram*, 8909
- Conley, A., Howell, D. A., Howes, A., et al. 2006, *AJ*, 132, 1707
- Courtois, H. M., & Tully, R. B. 2015, *MNRAS*, 447, 1531
- Dekker, H., D’Odorico, S., Kaufer, A., Delabre, B., & Kotzlowski, H. 2000, in *Proc. SPIE*, Vol. 4008, Optical and IR Telescope Instrumentation and Detectors, ed. M. Iye & A. F. Moorwood, 534–545
- Dessart, L., Blondin, S., Hillier, D. J., & Khokhlov, A. 2014, *MNRAS*, 441, 532
- Dhawan, S., Leibundgut, B., Spyromilio, J., & Blondin, S. 2016, *A&A*, 588, A84
- Faber, S. M., Phillips, A. C., Kibrick, R. I., et al. 2003, in *Proc. SPIE*, Vol. 4841, Instrument Design and Performance for Optical/Infrared Ground-based Telescopes, ed. M. Iye & A. F. M. Moorwood, 1657–1669
- Fitzpatrick, E. L. 1999, *PASP*, 111, 63
- Foley, R. J., Challis, P. J., Filippenko, A. V., et al. 2012, *ApJ*, 744, 38
- Fox, O. D., Kutyrev, A. S., Rapchun, D. A., et al. 2012, in *Proc. SPIE*, Vol. 8453, High Energy, Optical, and Infrared Detectors for Astronomy V, 845310

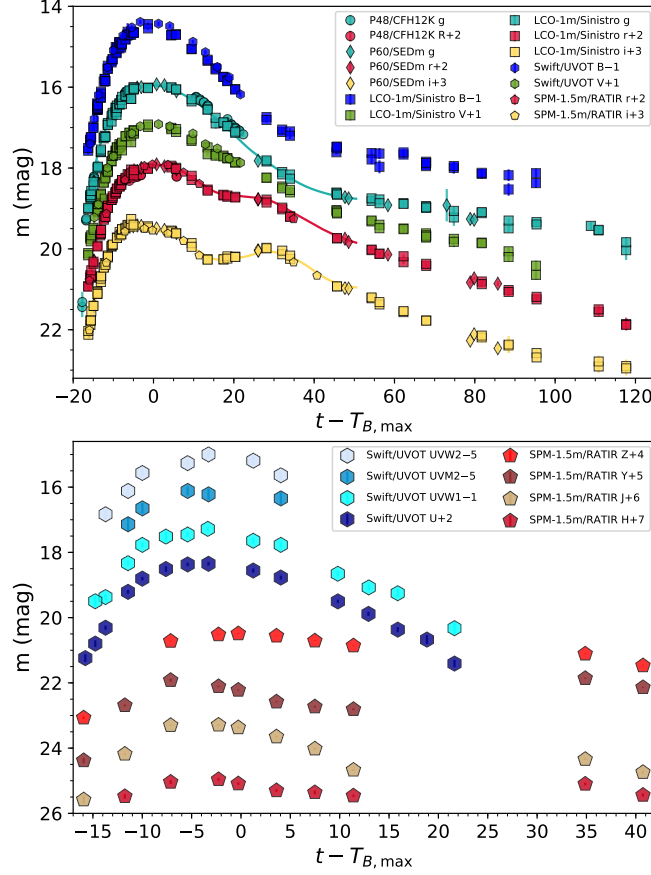


**Figure 9.** UV, optical, and NIR light curves for iPTF 16abc. *Top:* *BVgri* light curves from the P48, P60, and LCO-1m telescopes. The solid lines represent the best-fit model from SALT2 (see 3.3). *Bottom:* UV and NIR light curves from the *Swift* and SPM-1.5m telescopes, respectively. For both panels each light curve is represented with a different color, while the different symbols correspond to different instruments, as detailed in the legends. The legends also list offsets applied to each light curve. Photometry is shown in the AB mag system, with the exception of the *BV* bands, which are shown in the Vega system. The photometry shown has not been corrected for line-of-sight extinction.

Fremming, C., Sollerman, J., Taddia, F., et al. 2016, *A&A*, 593, A68  
 Ganeshalingam, M., Li, W., & Filippenko, A. V. 2011, *MNRAS*, 416, 2607  
 Goobar, A., Johansson, J., Amanullah, R., et al. 2014, *ApJL*, 784, L12  
 Goobar, A., Kromer, M., Siverd, R., et al. 2015, *ApJ*, 799, 106  
 Guy, J., Astier, P., Baumont, S., et al. 2007, *A&A*, 466, 11  
 Hayden, B. T., Garnavich, P. M., Kasen, D., et al. 2010a, *ApJ*, 722, 1691  
 Hayden, B. T., Garnavich, P. M., Kessler, R., et al. 2010b, *ApJ*, 712, 350  
 Hodgkin, S. T., Irwin, M. J., Hewett, P. C., & Warren, S. J. 2009, *MNRAS*, 394, 675  
 Hook, I. M., Jørgensen, I., Allington-Smith, J. R., et al. 2004, *PASP*, 116, 425  
 Hosseinzadeh, G., Sand, D. J., Valenti, S., et al. 2017, *ArXiv e-prints*, arXiv:1706.08990

Im, M., Choi, C., Yoon, S.-C., et al. 2015, *ApJS*, 221, 22  
 Kasen, D. 2010, *ApJ*, 708, 1025  
 Kromer, M., Fremming, C., Pakmor, R., et al. 2016, *MNRAS*, 459, 4428  
 Law, N. M., Kulkarni, S. R., Dekany, R. G., et al. 2009, *PASP*, 121, 1395  
 Levanon, N., Soker, N., & García-Berro, E. 2015, *MNRAS*, 447, 2803  
 Littlejohns, O. M., Butler, N. R., Cucchiara, A., et al. 2014, *AJ*, 148, 2  
 Maoz, D., Mannucci, F., & Nelemans, G. 2014, *ARA&A*, 52, 107  
 Marion, G. H., Sand, D. J., Hsiao, E. Y., et al. 2015, *ApJ*, 798, 39  
 Marion, G. H., Brown, P. J., Vinkó, J., et al. 2016, *ApJ*, 820, 92  
 Masci, F. J., Laher, R. R., Rebbapragada, U. D., et al. 2017, *PASP*, 129, 014002

- Miller, A. A., Laher, R., Masci, F., et al. 2016, *The Astronomer’s Telegram*, 8907
- Morozova, V., Piro, A. L., Renzo, M., et al. 2015, *ApJ*, 814, 63
- Noebauer, U. M., Kromer, M., Taubenberger, S., et al. 2017, *ArXiv e-prints*, arXiv:1706.03613
- Nugent, P. E., Sullivan, M., Cenko, S. B., et al. 2011, *Nature*, 480, 344
- Ofek, E. O., Laher, R., Surace, J., et al. 2012, *PASP*, 124, 854
- Oke, J. B., Cohen, J. G., Carr, M., et al. 1995, *PASP*, 107, 375
- Olling, R. P., Mushotzky, R., Shaya, E. J., et al. 2015, *Nature*, 521, 332
- Parrent, J. T., Thomas, R. C., Fesen, R. A., et al. 2011, *ApJ*, 732, 30
- Parrent, J. T., Howell, D. A., Friesen, B., et al. 2012, *ApJL*, 752, L26
- Phillips, M. M. 1993, *ApJL*, 413, L105
- Phillips, M. M., Simon, J. D., Morrell, N., et al. 2013, *ApJ*, 779, 38
- Piro, A. L., Chang, P., & Weinberg, N. N. 2010, *ApJ*, 708, 598
- Piro, A. L., & Morozova, V. S. 2016, *ApJ*, 826, 96
- Piro, A. L., & Nakar, E. 2014, *ApJ*, 784, 85
- Poznanski, D., Prochaska, J. X., & Bloom, J. S. 2012, *MNRAS*, 426, 1465
- Rabinak, I., & Waxman, E. 2011, *ApJ*, 728, 63
- Rahmer, G., Smith, R., Velur, V., et al. 2008, in *Proc. SPIE*, Vol. 7014, *Ground-based and Airborne Instrumentation for Astronomy II*, 70144Y
- Schlafly, E. F., & Finkbeiner, D. P. 2011, *ApJ*, 737, 103
- Shappee, B. J., Piro, A. L., Stanek, K. Z., et al. 2016a, *ArXiv e-prints*, arXiv:1610.07601
- Shappee, B. J., Piro, A. L., Holoien, T. W.-S., et al. 2016b, *ApJ*, 826, 144
- Silverman, J. M., & Filippenko, A. V. 2012, *MNRAS*, 425, 1917
- Silverman, J. M., Ganeshalingam, M., Cenko, S. B., et al. 2012, *ApJL*, 756, L7
- Skrutskie, M. F., Cutri, R. M., Stiening, R., et al. 2006, *AJ*, 131, 1163
- Taddia, F., Sollerman, J., Leloudas, G., et al. 2015, *A&A*, 574, A60
- Theureau, G., Hanski, M. O., Coudreau, N., Hallet, N., & Martin, J.-M. 2007, *A&A*, 465, 71
- Thomas, R. C., Aldering, G., Antilogus, P., et al. 2007, *ApJL*, 654, L53
- . 2011, *ApJ*, 743, 27
- Tonry, J. L. 2011, *PASP*, 123, 58
- . 2013, *Philosophical Transactions of the Royal Society of London Series A*, 371, 20120269
- Valenti, S., Howell, D. A., Stritzinger, M. D., et al. 2016, *MNRAS*, 459, 3939
- Vernet, J., Dekker, H., D’Odorico, S., et al. 2011, *A&A*, 536, A105
- Watson, A. M., Richer, M. G., Bloom, J. S., et al. 2012, in *Proc. SPIE*, Vol. 8444, *Ground-based and Airborne Telescopes IV*, 84445L
- Whelan, J., & Iben, Jr., I. 1973, *ApJ*, 186, 1007
- Zacharias, N., Finch, C. T., Girard, T. M., et al. 2013, *AJ*, 145, 44
- Zhang, K., Wang, X., Zhang, J., et al. 2016, *ApJ*, 820, 67
- Zheng, W., Silverman, J. M., Filippenko, A. V., et al. 2013, *ApJL*, 778, L15
- Zheng, W., Shivvers, I., Filippenko, A. V., et al. 2014, *ApJL*, 783, L24